Phys. Status Solidi A **212**, No. 12, 2747–2753 (2015) / **DOI** 10.1002/pssa.201532385

physica status solidi a
www.pss-a.com
applications and materials science

Influence of side groups on the performance of infrared absorbing aza-BODIPY organic solar cells

Stefan Kraner[*,1], Johannes Widmer[1], Johannes Benduhn[1], Ellen Hieckmann[2], Till Jägeler-Hoheisel[1], Sascha Ullbrich[1], Daniel Schütze[1], K. Sebastian Radke[4,5], Gianaurelio Cuniberti[3,4,5], Frank Ortmann[3,4], Melanie Lorenz-Rothe[1], Rico Meerheim[1], Donato Spoltore[1], Koen Vandewal[1], Christian Koerner[1], and Karl Leo[1]

[1] Institut für Angewandte Photophysik, Technische Universität Dresden, 01062 Dresden, Germany
[2] Institut für Angewandte Physik, Technische Universität Dresden, 01069 Dresden, Germany
[3] Institute for Materials Science and Max Bergmann Center of Biomaterials, 01062 Dresden, Germany
[4] Dresden Center of Computational Materials Science, Technische Universität Dresden, 01062 Dresden, Germany
[5] Center for Advancing Electronics Dresden, Technische Universität Dresden, 01062 Dresden, Germany

Received 11 May 2015, revised 3 July 2015, accepted 3 Jul 2015
Published online 25 July 2015

Keywords organic solar cells, infrared absorbers, side groups, electron transfer losses, traps, aza-BODIPY

[*] Corresponding author: e-mail stefan.kraner@iapp.de, Phone: +49-351-463-35117, Fax: +49-351-463-37065

Organic solar cells are a promising technology for a large area conversion of sunlight into electricity. In particular for solar cells based on oligomers (small molecules), efficient donor materials absorbing wavelengths larger than 780 nm are still rare. Here, we investigate three aza-BODIPY dyes absorbing in the infrared. The addition of side groups leads to a red shift of the optical gap from 802 to 818 nm. In optimized devices using these donors in a bulk heterojunction with C_{60}, we observe a higher charge carrier mobility and a higher power conversion efficiency for the molecules without a methyl or methoxy side group lowering the molecular reorganization energy. Surprisingly, the donor–acceptor blend with the lowest energy loss during the electron transfer to the C_{60} yields the highest short circuit current. With increasing size of the attached side chain, the devices exhibit a larger trap density, measured by impedance spectroscopy. Based on the investigation of different blend ratios, we conclude that these traps are mainly present in the donor phase.

1 Introduction Organic photovoltaics (OPV) is a promising technology for low cost energy supply. In the last 5 years, the power conversion efficiency (PCE) has doubled and reaches about 12% for both small molecule and polymer solar cells [1–3]. These record efficiencies were achieved with tandem or triple solar cells, where different donor materials are used to absorb complementary parts of the solar spectrum. In the visible part of the solar spectrum, efficient solar cells with PCE of almost 10% have been reported [4, 5]. In the near infrared (NIR) regime, there is still a significant potential to improve the overall power conversion, in particular for solar cells based on oligomers (small molecules), if efficient NIR absorbing materials can be synthesized. Among the different molecular structures investigated, the class of benzannulated 4,4-difluoro-4-bora-3a,4a-diaza-s-indacene (aza-BODIPY) was reported as an interesting NIR absorber and electron donor class for OPV devices [6–9].

In this work, we investigate in details the properties of three aza-BODIPY molecules with different side chains attached and prepare optimized solar cells. The molecules show excellent absorption characteristics in the NIR spectral range [6]. The optimized solar cell stacks (Fig. 1) are characterized by current–voltage (IV) measurements as well as external and internal quantum efficiency (EQE, IQE) measurements. In order to understand the differences in the open-circuit voltage (V_{OC}), we performed temperature dependent V_{OC} measurements to obtain the effective gap ($e \cdot V_0$) of the blend used. Furthermore, we determine the charge carrier mobilities by open-circuit corrected charge carrier extraction (OTRACE) in the donor–acceptor blends and measure the trap densities by impedance spectroscopy.

We obtain a maximum PCE of 3.8% and for NIR absorber a remarkable V_{OC} of 0.81 V for the device using Ph_2-benz-BODIPY as a donor. When adding a methyl group to

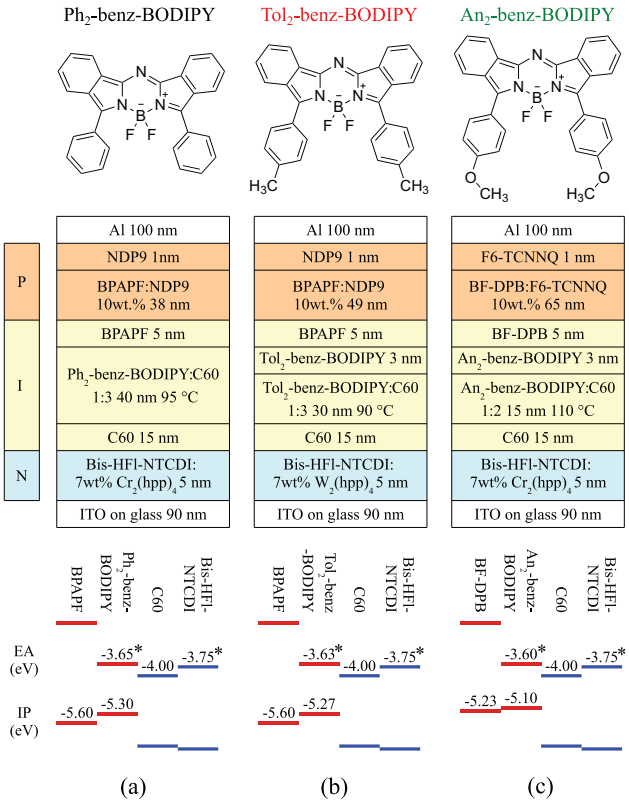

Figure 1 Top: (a) Ph_2-benz-BODIPY, (b) Tol_2-benz-BODIPY, (c) An_2-benz-BODIPY. Middle: Optimized solar cell stack for each material shown above. Bottom: Ionization potential (IP) and electron affinity (EA) or LUMO (from CV denoted by * [6]) for the used organic materials. For more information see text.

the Ph_2-benz-BODIPY, the aza-BODIPY solar cells exhibit a lower PCE, IQE, short-circuit current density (j_{SC}), fill factor (FF) and V_{OC}. Attaching a methoxy group further decreases these values. The lower V_{OC} can be explained by a lower effective gap of the used heterojunction. Contrary to expectations, an increased j_{SC} for the devices with a lower electron energy loss from the donor to the acceptor is observed. The decrease of j_{SC} with larger side chains can be attributed to a lower charge carrier mobility and a higher trap density. The former can be explained by density functional theory (DFT) calculations, showing a higher reorganization energy for the aza-BODIPYs with longer side chains. Based on impedance spectroscopy investigations on various solar cell stacks and donor–acceptor blend ratios, we conclude that the traps are present in the donor, where they might act as recombination centers for excitons. Finally, we investigated the morphology of the blends by grazing incidence X-ray diffraction (GIXRD) and scanning electron microscopy (SEM). The measurements show that there is no significant difference between the layers made by the different molecules.

2 Experimental and computational details

Prior to use, all materials, except the dopants, were purified by vacuum gradient sublimation. The solar cells were produced by thermal evaporation in vacuum with shadow masks and at a base pressure of 10^{-8} mbar (K. J. Lesker, UK) on prestructured indium tin oxide (ITO) (Thin Film Devices, USA). The substrates were cleaned by a multistep wet process. Doped and blend layers are fabricated by co-evaporation of two materials. The device area is defined by the overlap of the indium tin oxide (ITO) and the aluminum top layer evaporated with a shadow mask and is 6.44 mm^2. To ensure long device lifetime, all devices were encapsulated with a glass cavity.

The external quantum efficiency is determined using the lock-in technique with a monochromator (Cornerstone 260), a xenon arc-lamp and lock-in amplifier (7265 DSP Signal Recovery). This technique is used for the absolute determination of the EQE values.

Current voltage characteristics are measured by a Keithley 2400 under a simulated AM 1.5G sun light (16 S-150 V.3 Solar Light) at a spectral mismatch (MM) corrected light intensity.

The internal quantum efficiency is calculated from the ratio of EQE and absorption of the intrinsic layers, where the absorption of the intrinsic layers is simulated by the software Osolemio, which is based on a transfer-matrix-formalism [28]. In order to lower deviations between simulated and measured absorption, the total absorption of the stack is measured in a home-made reflection setup with an Ava-Light-DH-S-Bal (Avantes BV, Netherlands) light source and a spectrometer (OMT reflection measuring system). The simulated total absorption is then adjusted to the measured total absorption by an adjustment factor. The adjustment factor is used to correct the simulation of the absorption of the intrinsic layers. The adjustment factor covers optical effects which are not included in the one-dimensional simulations, i.e., high roughness at the donor–acceptor interface. We observe the highest deviations for the blends with largest grains (see SEM images in the Supporting Information, online at: www.pss-a.com). The index of refraction n and the extinction coefficient k, which are required for simulation, have been modeled from absorption and reflection measurements on thin films with varying thicknesses. Reflection and absorption were measured with a two-beam spectrometer UV 3100 Shimadzu Corporation. The absorption obtained for the intrinsic layers of the respective device is shown in the Supporting Information.

The OTRACE setup consists of an Oscilloscope (Tektronix DPO 7354C) and a waveform generator (Agilent 33622A). The sample is illuminated with a white LED (Luxeon K2) with an intensity of about 100 mW/cm^2 in steady state conditions. Upon turning off the LED a time dependent offset voltage is applied to the device to avoid the sweep-out of charge carriers. After a delay time, a ramp voltage is applied on the sample to extract the remaining charge carriers [17]. All curves are measured with the same ramp voltage A' (1 V/40 µs) after a delay time (t_{del} = 1 µs).

Impedance measurements are performed with an Autolab PGSTAT302N. For the probe signal an amplitude of 20 mV with zero DC bias is used. For the temperature regulation a cryostat with a Peltier element (HAT belektroniG) is used.

The stacks used for impedance and OTRACE analysis are optimized for the specific measurement technique and therefore differ slightly from the stacks shown in Fig. 1. For more information about the used stacks, see Supporting Information.

In the temperature dependent measurement, the V_{OC} is measured with a source measure unit (Keithley 2400). It is interpolated from the two points of the current–voltage characteristic where the sign of the current density changes. The current–voltage characteristic is taken with a step-width of 50 mV. The accuracy is better than $\Delta V_{OC} \approx 30$ mV. For temperature variation, the sample is mounted onto a temperature controlled copper block in vacuum, differences due to a temperature gradient in the substrate between temperature sensor and the active sample area are corrected by prior calibration. The sample is illuminated by a white light LED [15].

GIXRD measurements are carried out on a Bruker D8 Discover diffractometer. A 3rd generation 60 mm Göbel mirror is used to parallelize Cu Kα radiation from a X-ray tube operated at 40 kV and 40 mA. The angle of incidence is set to the critical angle for total external reflection ($\omega \sim 0.2^\circ$). The diffracted intensity depending on the detector angle is collected in the range between 3° and 90° with a step size of 0.1° and 30 s sampling time per step. For the separation of the background a second measurement is carried out in the same 2θ range at an angle of incidence below the critical angle ($\omega \approx 0.1^\circ$). For GIXRD measurements, we use glass substrates with 70 nm blend, evaporated at the specified substrate temperature and in the optimized ratio.

Based on density functional theory (DFT) calculations, we obtain the reorganization energy for hole transfer by $\lambda_+ = [E_0(q_+) - E_0(q_0)] + [E_+(q_0) - E_+(q_+)]$, with $E_0(q_+)$ the energy of the neutral molecule in the equilibrium geometry of the cation q_+, $E_0(q_0)$ the equilibrium energy of the neutral molecule, $E_+(q_0)$ the energy of the cation in the equilibrium geometry of the neutral state q_0, and $E_+(q_+)$ the equilibrium energy of the cation [29]. All calculations are performed by using the Gaussian09 suite [30] in combination with the B3LYP exchange-correlation functional [31] and the 6-311G(d,p) basis set [32].

3 Results In our study, the donor absorber materials (Fig. 1) are varied. Since C_{60} is used as acceptor material, the electron transport material is the same for all three stacks, i.e., *N,N*-bis(fluoren-2-yl)-naphthalenetetracarboxylic diimide (Bis-HFl-NTCDI) [10] doped with tetrakis(1,3,4,6,7,8-hexahydro-2*H*-pyrimido[1,2-*a*]pyrimidinato)dichromium(II) ($Cr_2(hpp)_4$) or tetrakis(1,3,4,6,7,8-hexahydro-2*H*-pyrimido [1,2-*a*] pyrimidinato)ditungsten (II) ($W_2(hpp)_4$) [11]. The two different n-dopants do not significantly affect the device performance. An intrinsic C_{60} layer on the n-side with a thickness of 15 nm avoids direct contact of the excitons created in the donor material with the n-dopant in the transport layer reducing recombination losses. The parameters to be optimized for the bulk heterojunction are the thickness of the donor–acceptor blend, the mixing ratio, and the substrate temperature during evaporation. The adjusted parameters are shown in Fig. 1. For Tol_2-benz-BODIPY (b) and An_2-benz-BODIPY (c), an additional neat donor layer of 3 nm increases the absorption, the short-circuit current density and the PCE, while in Ph_2-benz-BODIPY devices an additional pure layer increases the absorption but lowers the fill factor to a certain degree, which leads to lower PCE compared to devices without a neat donor layer.

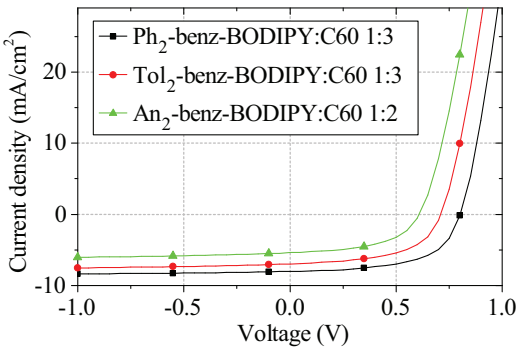

Figure 2 Current–voltage characteristics of optimized aza-BODIPY devices under mismatch corrected AM 1.5G illumination.

The electron affinity or lowest unoccupied molecular orbital (LUMO) values shown in Fig. 1 at the bottom are measured via inverse photoelectron spectroscopy (IPES) for C_{60} [12] and from cyclic voltammetry (CV) [6] for the aza-BODIPYs and Bis-HFl-NTCDI, respectively. All ionization potentials (IP) are obtained by ultraviolet photoelectron spectroscopy (UPS) [13]. The IP of the hole transport material 9,9-bis[4-(*N,N*-bis-biphenyl-4-yl-amino)phe-nyl]-9H-fluorene (BPAPF) is about 0.3 eV below the IP of the donor material, which should in principle act as a hole extraction barrier. Notwithstanding, no s-kink can be observed and the charge extraction is most efficient with the chosen hole transport material. For the An_2-benz-BODIPY donor material, the IP of BPAPF is too low, and *N*, *N*′-((Diphenyl-*N*, *N*′-bis)-9,9-dimethyl-fluoren-2-yl)-benzidine (BF-DPB) is used instead. BPAPF is doped with a commercially available dopant (NDP9 from Novaled) and BF-DPB with 2, 2′-(per-fluoronaph-thalene-2,6-diylidene) dimalononitrile (F6-TCNNQ). To prevent exciton recombination on the p-side, an additional layer of the undoped hole transport material with a thickness of 5 nm is added between the donor-acceptor blend and the p-doped transport layer.

Figure 2 shows the IV curves from devices introduced, whereas Table 1 presents the IV-characteristics obtained. Overall, we get the best performance for Ph_2-benz-BODIPY with a PCE of 3.8% for the material without a side group, i.e., Ph_2-benz-BODIPY. The PCE decreases with methyl substitution (Tol_2-benz-BODIPY) and even more in the case of methoxy substitution (An_2-benz-BODIPY). This trend is valid for all investigated physical parameters. Hence, attaching methyl or methoxy groups leads to a lower PCE, j_{SC}, FF, V_{OC}, charge carrier mobility (μ) and higher trap densities.

The open-circuit voltage is determined by the effective gap and by the recombination of generated charges. The effective gap can be obtained by the difference of ionization

Table 1 Electrical properties from IV measurements, measured mobility μ, calculated reorganization energy λ_+, the measured energetically trap depth with their densities, measured effective gap eV_0 and measured optical gap $E_{g_{opt}}$ for the 3 optimized BODIPY devices (see Fig. 1). For more information see text. IV curves are shown in the Supporting Information.

	Ph_2-benz-BODIPY device	Tol_2-benz-BODIPY device	An_2-benz-BODIPY device	Units
PCE	3.8	2.7	1.7	%
j_{SC}	8.0	7.0	5.4	mA/cm^2
FF	59	55	52	%
V_{OC}	0.81	0.71	0.61	V
μ	15	7.4	4.0	10^{-6} cm^2/Vs
λ_+	139	159	231	meV
trap depth		0.33	0.34	eV
trap density		0.4	1.0	10^{16} cm^{-3}
eV_0	1.38	1.22	1.14	$\pm$ 0.06 eV
$E_{g_{opt}}$	1.55	1.55	1.52	$\pm$ 0.02 eV

potential of the donor and the electron affinity of the acceptor, which is 4 eV for C_{60} [12], see Fig. 1(bottom). The IP values of the donor are measured on pure materials by ultraviolet photoelectron spectroscopy (UPS). Since, the IP can also be a function of the mixing ratio with C_{60} [14], we perform temperature dependent V_{OC} measurements to obtain the effective gap for the donor–acceptor blends used [15]. Extrapolating V_{OC} to 0 K gives V_0, corresponding to the energy eV_0. Temperature dependent V_{OC} measurements are performed at different illumination intensities and are shown in the Supporting Information, while the obtained mean values are given in Table 1. eV_0 agrees very well with energetic difference between the IP of the donor and the EA of the acceptor (from Fig. 1). Based on the V_0 measurement, the effective gap has the same trend as V_{OC} and is 0.51–0.57 V higher compared to respective V_{OC} at ambient temperature. Hence, the difference in V_{OC} for the different donors can be explained by the differences in the effective gaps of the investigated donor–acceptor blends.

The optical gap can be determined by the intersection of the normalized absorption and emission spectrum [16]. Using the measured optical gap of 1.55 eV for Ph_2-benz-BODIPY and Tol_2-benz-BODIPY and 1.52 eV for An_2-benz-BODIPY (see Supporting Information), we obtain a difference between the effective (eV_0) and the optical gap ($E_{g_{opt}}$) of 0.17, 0.33, and 0.38 eV for Ph_2-benz-BODIPY, Tol_2-benz-BODIPY and An_2-benz-BODIPY, respectively (see also Table 1). This difference, reflecting the driving force for an electron transfer from the singlet state (donor) into the CT-state (donor–acceptor), is smallest for the best performing device and therefore seems to have a minor influence for an efficient charge carrier separation.

In Fig. 3 the extinction coefficients (k) of the three blend layers are shown. The values of the An_2-benz-BODIPY are highest and the spectrum is slightly more red shifted. The increased absorption can mainly be attributed to a higher optimized mixing ratio of 1:2, compared to 1:3, yielding more

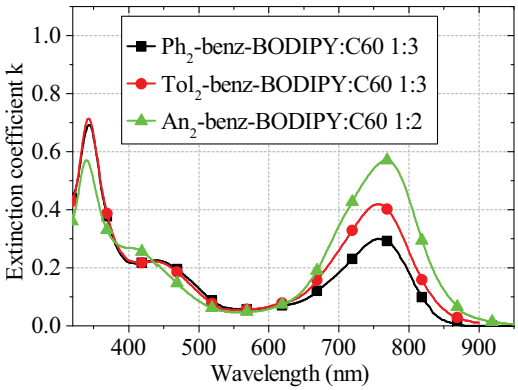

Figure 3 Extinction coefficient k of the three aza-BODIPYs mixed with C_{60} in their optimized ratio and evaporated at the optimized substrate temperature (see Fig. 1).

absorber molecules in the blend. The Ph_2-benz-BODIPY exhibits the lowest extinction coefficient. Between 300 and 500 nm, all three blends show an additional contribution to the absorption related to the C_{60}. Despite the higher extinction coefficient and lower film thicknesses for the blends consisting of donor molecules with methyl and methoxy groups, the FF of these optimized devices is lower compared to devices based on the Ph_2-benz-BODIPY. In Fig. 4 the external quantum efficiencies (EQE) and the internal quantum efficiencies (IQE) of the optimized stacks are shown. The maximum of the EQE in the NIR part of the spectrum are similar (0.38–0.41). The higher extinction coefficient of the An_2-benz-BODIPY blend does not lead to a higher EQE. The IQE is similar for the An_2-benz-BODIPY and Tol_2-benz-BODIPY devices, whereas for the Ph_2-benz-BODIPY device, the IQE is higher over the entire spectral range with a maximum close to unity in the NIR part, indicating a very efficient exciton dissociation and extraction process. The optimized devices exhibit different blend thicknesses, leading to a higher EQE for the devices with a thicker blend layer between the wavelengths 300 and 550 nm, reflecting the higher amount of C_{60} in the blend.

In order to understand the reason for the higher IQE and FF, the OTRACE technique is used to determine the mobility

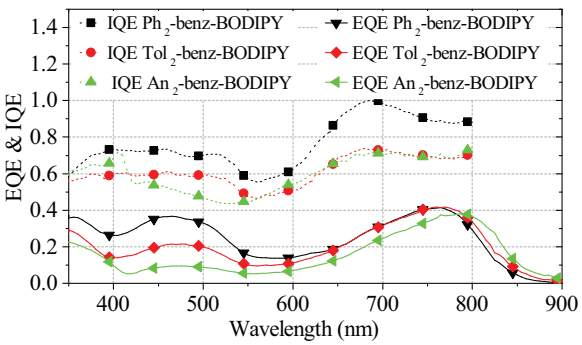

Figure 4 External quantum efficiency (EQE) and internal quantum efficiency (IQE) of optimized aza-BODIPY solar cells (see Fig. 1).

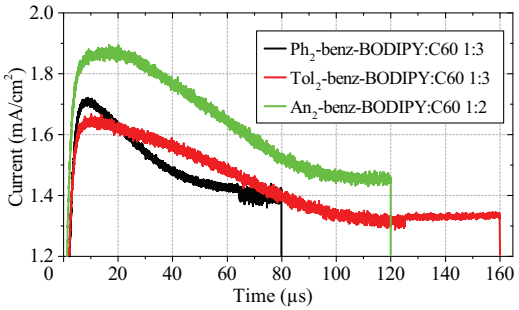

Figure 5 Current transient measured with the OTRACE technique on the three aza-BODIPY materials. The ramp ($A' = 1$ V/40 µs) and the delay time ($t_{del} = 1$ µs) is the same for all curves, only the extraction time is different (80, 120, or 160 µs).

of the photogenerated charge carriers [17]. In Fig. 5 the extracted transient curves from the three aza-BODIPY derivatives are shown. To calculate the mobility, we use the equation derived by Lorrmann et al. [18]. For the charge carrier mobility the same trend as for the PCE is observed (see Table 1), i.e. an increasing mobility ($4 \times 10^{-6} \rightarrow 7.4 \times 10^{-6} \rightarrow 15 \times 10^{-6}$ cm^2/Vs) enables thicker donor–acceptor blends (15 nm → 30 nm → 40 nm), which absorb more light and therefore increase the PCE. The charge carrier mobilities measured with OTRACE should, however, be taken with caution, since traps present influence the charge extraction and are not considered in the derivation of the used equation [18]. Furthermore, one can not distinguish between hole and electron mobility. The charge carrier mobility can be affected by intrinsic or extrinsic effects. Intrinsic properties are determined by the molecule or material itself, such as the internal reorganization energy λ_+ of a molecule [19, 20]. Table 1 presents λ_+ calculated by DFT. We consistently calculate a lower reorganization energy for the aza-BODIPYs with a higher charge carrier mobility. Since, the crystallinity of the different donor–acceptor blends is similar (see Supporting Information), a change of the mobility due to a different degree of crystallization in the donor can be excluded. Notwithstanding, intermolecular interactions can additionally affect the charge transport, which are not covered in this investigation.

Extrinsic reasons affecting the charge carrier mobility can be traps caused by impurities or structural defects [21, 22]. Thus, we perform temperature and frequency dependent capacitance measurements to obtain the trap densities and their energetic position shown in Fig. 6 [23, 24]. These spectra show the capacitance measured between 100 and 10^6 Hz. In the Tol$_2$-benz-BODIPY and An$_2$-benz-BODIPY devices ((b), (c), and (d) of Fig. 6, a contribution to the capacitance can be detected at about 20 kHz. This additional capacity can be attributed to a trap capacity. Following the theory of Walter et al. [23, 24], we use the capacitance spectra to calculate the density of states (DOS) of the traps shown in Fig. 6(f)–(h). The depletion width required for the calculation is determined by the thickness of the intrinsic layer shown in Fig. 1, while the built-in potential, and accordingly the Fermi-level difference between the hole and the electron transport layer, is estimated to be 1.45, 1.45, and 1.08 V for Ph$_2$-benz-BODIPY, Tol$_2$-benz-BODIPY, and An$_2$-benz-BODIPY devices, respectively, thus the Fermi-level is taken to be 0.2 eV lower than the electron transport level and 0.2 eV higher than hole transport level (see Fig. 1). Since the built-in potential only scales the amplitude of the DOS, for the sake of comparison the assumptions made are reasonable. The resulting Arrhenius plots giving the attempt to escape frequencies ν and the activation energies E_A are shown in Fig. 6(e). The activation energy E_A represents the energy

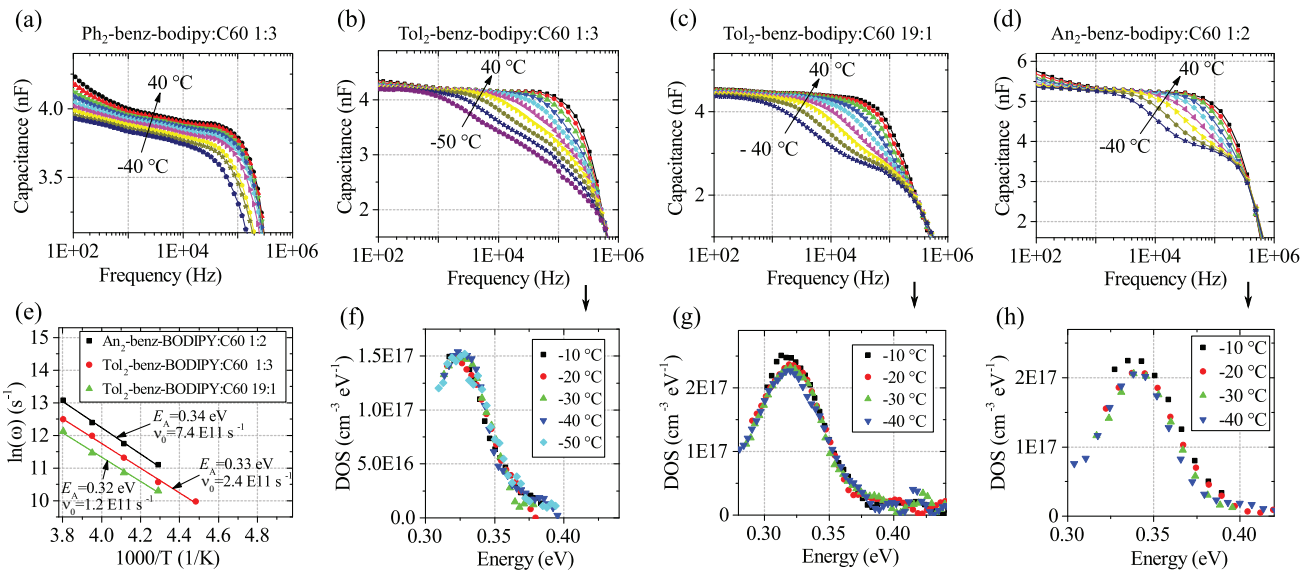

Figure 6 (a)–(d) Measured capacitance spectra for the three aza-BODIPY devices, including a donor dominated mixing ratio of 19:1. In (b),(c) and (d) trap contributions can be detected. (e) Arrhenius plot of the inflections points derived from the capacitance spectra. (f)–(h) DOS of traps reconstructed from the capacitance spectra above.

difference between the conduction or valence band and the trap energy (trap depth). The trap densities are represented by the area below the curve of the DOS and are listed in Table 1. In the device with Ph_2-benz-BODIPY donor molecules, no trap density could be identified, whereas replacing the donor with the Tol_2-benz-BODIPY donor material leads to an additional trap capacitance (Fig. 6(b) and (f)) with trap depth of 0.33 eV and a density of $0.4 \times 10^{16}\,cm^{-3}$. For the device based on An_2-benz-BODIPY (Fig. 6(d)and (h)) the trap density increases to $1.0 \times 10^{16}\,cm^{-3}$, while the trap depth does only change within the measurement error. Thus, the traps are related to the donor material or the interface between the donor and the acceptor.

Figure 6(c) shows the trap capacitance spectra of a Tol_2-benz-BODIPY device with a donor–acceptor blend ratio of 19 to 1. We obtain a similar trap energy as in the optimized blend (≈0.33 eV), but the trap density increases from 0.4 to 1.48×10^{16} cm^{-3}, see DOS plot in Fig. 6(f) and (g). If the traps are located at the donor–acceptor interface, the DOS would decrease with a larger amount of donor in the blend since the interface area does decrease, which is not observed. We therefore conclude that the traps are present in the donor material [25]. Traps from structural defects usually exhibit states into the gap by an exponential behavior [26], while traps with a distinct level in the gap, as observed here, can be attributed to chemical defects [27]. Therefore, we conclude that longer side chains induce more chemical defects in the BODIPY devices investigated. During evaporation the molecule (especially the attached side groups) could break, leading to new HOMO and LUMO energies, which might act as traps. The temperature of the crucible during evaporation is 185, 196, and 207 °C for the Ph_2-benz-BODIPY, Tol_2-benz-BODIPY and An_2-benz-BODIPY, respectively. The material needing the highest crucible temperature for an evaporation rate of 0.3 Å/s exhibits the highest amount of traps.

4 Conclusion In their optimized solar cell stack, the three aza-BODIPYs show a PCE of 3.8, 2.7, and 1.7% for Ph_2-benz-BODIPY, Tol_2-benz-BODIPY and An_2-benz-BODIPY, respectively. The device with the highest short circuit current exhibits the lowest energy losses for the electron transfer from the donor to the acceptor (≈0.17 eV), indicating that for efficient charge extraction a large driving force for electron transfer is not necessary. The trend in the PCE correlates with a higher charge carrier mobility measured by OTRACE. The mobility decreases with increasing size of the functional group. The differences in the mobilities can be explained by a lower reorganization energy of the donor molecule and by an increasing amount of traps. Using impedance spectroscopy, a higher trap density can be measured for the lower performing aza-BODIPY blends. Furthermore, we observe an increase of the trap density for a higher amount of donor molecules in the blend. Hence, the traps originate from the bulk of the donor. We conclude that for the used aza-BODIPY dyes the additional side groups lower the charge carrier mobilities due to a higher reorganization energy and an increased trap density in the donor material, leading to a lower power conversion efficiency.

Supporting Information Additional supporting information may be found in the online version of this article at the publisher's website.

Acknowledgements The author would like to thank Dr. Lutz Wilde for performing GIXRD measurements at the Fraunhofer CNT in Dresden and Roland Gresser for the synthesis of the An_2-benz-BODIPY. This work was financially supported by the German Bundesministerium für Bildung und Forschung (BMBF) under the contract No. FKZ 03EK3505D (LOTsE project), 03EK3503A (MEDOS project) and the INNO-PROFILE project 03IPT602X "Organische p-i-n Bauelemente 2.2". We further gratefully acknowledge support from the German Excellence Initiative via the Cluster of Excellence EXC 1056 "Center for Advancing Electronics Dresden" (cfAED). Additionally, this work was partially supported by the Heinrich Böll Stiftung e.V. and the DFG (OR 349/1-1). Computational resources were provided by the Center for Information Services and High Performance Computing (ZIH) of Dresden University of Technology.

References

[1] A. R. B. Mohd Yusoff, D. Kim, H. P. Kim, F. K. Shneider, W. J. da Silva, and J. Jang, Energy Environ. Sci. **8**, 303–316 (2014).
[2] www.heliatek.com, accessed March 2015.
[3] M. A. Green, K. Emery, Y. Hishikawa, W. Warta, and E. D. Dunlop, Progr. Photovolt. Res. and Appl. **23**(1), 1–9 (2015).
[4] Z. He, C. Zhong, S. Su, M. Xu, H. Wu, and Y. Cao Nature Photon. **6**, 591–595 (2012).
[5] R. Meerheim, C. Körner, and K. Leo, Appl. Phys. Lett. **105**(6), 063306 (2014).
[6] R. Gresser, M. Hummert, H. Hartmann, K. Leo, and M. Riede, Chem. Euro. J. **17**(10), 2939–2947 (2011).
[7] S. Y. Leblebici, L. Catane, D. E. Barclay, T. Olson, T. L. Chen, and B. Ma, ACS Appl. Mater. Interf. **3**(11), 4469–74 (2011).
[8] J. Meiss, F. Holzmueller, R. Gresser, K. Leo, and M. Riede, Appl. Phys. Lett. **99**(19), 193307 (2011).
[9] T. Mueller, R. Gresser, K. Leo, and M. Riede, Sol. Energy Mater. Sol. Cells **99**, 176–181 (2012).
[10] M. L. Tietze, F. Wölzl, T. Menke, A. Fischer, M. Riede, K. Leo, and B. Lüssem, Phys. Status Solidi A **210**(10), 2188–2198 (2013).
[11] F. A. Cotton, J. P. Donahue, D. L. Lichtenberger, C. A. Murillo, and D. Villagrán, J. Am. Chem. Soc. **127**(31), 10808–10809 (2005).
[12] W. Zhao and A. Kahn, J. Appl. Phys. **105**(12), 3711 (2009).
[13] S. Olthof, W. Tress, R. Meerheim, B. Lüssem, and K. Leo, J. Appl. Phys. **106**(10), 103711 (2009).
[14] M. L. Tietze, W. Tress, S. Pfützner, C. Schünemann, L. Burtone, M. Riede, K. Leo, K. Vandewal, S. Olthof, P. Schulz, and A. Kahn, Phys. Rev. B **88**(8), 085119 (2013).
[15] J. Widmer, M. Tietze, K. Leo, and M. Riede, Adv. Funct. Mater. **23**(46), 5814–5821 (2013).
[16] J. Gierschner, J. Cornil, and H. J. Egelhaaf, Adv. Mater. **19**(2), 173–191 (2007).
[17] A. Baumann, J. Lorrmann, D. Rauh, C. Deibel, and V. Dyakonov, Adv. Mater. **24**(32), 4381–6 (2012).

[18] J. Lorrmann, B. H. Badada, O. Inganäs, V. Dyakonov, and C. Deibel, J. Appl. Phys. **108**(11), 113705 (2010).
[19] F. Ortmann, F. Bechstedt, and K. Hannewald, Phys. Rev. B **79**(23), 235206 (2009).
[20] K. S. Radke, R. Scholz, F. Ortmann, K. Leo, and G. Cuniberti, J. Phys. Chem. C **118**, 6537–6547 (2014).
[21] L. Burtone, J. Fischer, K. Leo, and M. Riede, Phys. Rev. B **87**(4), 045432 (2013).
[22] J. Schafferhans, A. Baumann, A. Wagenpfahl, C. Deibel, and V. Dyakonov, Org. Electron. **11**(10), 1693–1700 (2010).
[23] S. Khelifi, K. Decock, J. Lauwaert, H. Vrielinck, D. Spoltore, F. Piersimoni, J. Manca, A. Belghachi, and M. Burgelman, J. Appl. Phys. **110**(9), 094509 (2011).
[24] T. Walter, R. Herberholz, C. Müller, and H. W. Schock, J. Appl. Phys. **80**(8), 4411–4420 (1996).
[25] The trap capacity also appears in An2-benz-BODIPY devices without a neat donor layer, as in the devices with Ph2-benz-BODIPY, thus it's origin is not only the neat layer.
[26] R. Noriega, J. Rivnay, K. Vandewal, F. P. V. Koch, N. Stingelin, P. Smith, M. F. Toney, and A. Salleo, Nature Mater. **12**(11), 1038–44 (2013).
[27] L. G. Kaake, P. F. Barbara, and X. Y. Zhu, J. Phys. Chem. Lett. **1**(3), 628–635 (2010).
[28] E. Centurioni, Appl. Opt. **44**(35), 7532–7539 (2005).
[29] V. Coropceanu, J. Cornil, D. A. da Silva Filho, Y. Olivier, R. Silbey, and J. L. Brédas, Chem. Rev. **107**(4), 926–952 (2007).
[30] M. J. Frisch, G. W. Trucks, H. B. Schlegel, G. E. Scuseria, M. A. Robb, J. R. Cheeseman, G. Scalmani, V. Barone, B. Mennucci, G. A. Petersson, H. Nakatsuji, M. Caricato, X. Li, H. P. Hratchian, A. F. Izmaylov, J. Bloino, G. Zheng, J. L. Sonnenberg, M. Hada, M. Ehara, K. Toyota, R. Fukuda, J. Hasegawa, M. Ishida, T. Nakajima, Y. Honda, O. Kitao, H. Nakai, T. Vreven, J. A. Montgomery Jr., J. E. Peralta, F. Ogliaro, M. Bearpark, J. J. Heyd, E. Brothers, K. N. Kudin, V. N. Staroverov, R. Kobayashi, J. Normand, K. Raghavachari, A. Rendell, J. C. Burant, S. S. Iyengar, J. Tomasi, M. Cossi, N. Rega, J. M. Millam, M. Klene, J. E. Knox, J. B. Cross, V. Bakken, C. Adamo, J. Jaramillo, R. Gomperts, R. E. Stratmann, O. Yazyev, A. J. Austin, R. Cammi, C. Pomelli, J. W. Ochterski, R. L. Martin, K. Morokuma, V. G. Zakrzewski, G. A. Voth, P. Salvador, J. J. Dannenberg, S. Dapprich, A. D. Daniels, O. Farkas, J. B. Foresman, J. V. Ortiz, J. Cioslowski, and D. J. Fox, Gaussian 09 Revision D.01.
[31] A. D. Becke, J. Chem. Phys. **98**(7), 5648–5652 (1993).
[32] R. Krishnan, J. S. Binkley, R. Seeger, and J. A. Pople, J. Chem. Phys. **72**(1), 650–654 (1980).